



Application of surfactant-modified zeolite-activated carbons as adsorbents to a semi-batch operation

Z. Ioannou*, C. Karasavvidis, A. Molla, A. Dimirkou

Soil Science Laboratory, Department of Agriculture, Crop Production and Rural Environment, University of Thessaly, Volos 38446, Magnesia, Greece, Tel. +30-24210-93287; Fax:+30-24210-93288; emails: zioan@teemail.gr (Z. Ioannou), chkarasavvidis@gmail.com (C. Karasavvidis), katrinmol@yahoo.gr (A. Molla), adimirkou@uth.gr (A. Dimirkou)

Received 4 August 2015; Accepted 23 January 2018

ABSTRACT

Modified zeolite-activated carbons (H-CL-CB1, H-CL-CB2) in a proportion of 50/50 w/w and 20/80 w/w were used for methylene blue removal from aqueous solutions under a semi-batch operation. Dye adsorption kinetic analysis was also studied for H-CL-CB1, H-CL-CB2, modified zeolite (H-CL), commercial activated carbon (CB), hematite (HM) and clinoptilolite (CL). Equilibrium isotherms and thermodynamic analysis of dye were studied for H-CL-CB1, H-CL-CB2, CB, CL, H-CL and HM under a batch operation at 20°C, 40°C and 60°C. The physical and chemical properties of all adsorbents were characterized through Fourier transform infrared spectroscopy, Brunauer–Emmett–Teller analysis and the point of zero charge. The maximum methylene blue removal (99% and 96%) on different modified zeolite-activated carbons (50/50 w/w and 20/80 w/w) was achieved after 57 and 130 min, respectively. Dye adsorption process onto H-CL and H-CL-CB1 (50/50 w/w) was found to be controlled by chemisorption while onto CB and H-CL-CB2 (20/80 w/w) by film diffusion. Isotherm studies have shown that dye adsorption data on CL, H-CL, H-CL-CB1 and H-CL-CB2 were best described by Freundlich isotherm while on HM and CB by Langmuir isotherm. According to thermodynamic study, the negative values of ΔG° indicate that dye adsorption process was favorable. The positive values of ΔH° indicate endothermic nature of adsorption. Zeolite-carbon adsorbents can be used as filters to remove organic compounds from wastewaters.

Keywords: Modified zeolite-activated carbon; Hematite; Modified zeolite; Methylene blue

1. Introduction

Dyes are among the most important sources of water pollution due to their non-biodegradable, teratogenic, carcinogenic and mutagenic nature. Colored effluents consist of a serious of environmental problem and even in low concentration are heavily colored, with high concentrations of salts and high biological/chemical oxygen demand [1]. It is estimated that more than 100,000 commercially available dyes with over 7×10^5 tons of dyestuff are produced annually [2].

Methylene blue (MB) is one of the most commonly used substances for dyeing cotton, wood and silk. It is a positively charged organic molecule, with high solubility to water [3]. Several techniques have been applied for dye removal such as coagulation–flocculation, membrane filtration, chemical precipitation, ion exchange and adsorption, which has received widespread attention over the last 15 years [4]. Although activated carbons are the best sorbent tools for the removal of dyes they can be replaced or combined by other low cost sorbents media such as zeolites, bentonites and iron oxides due to their high cost [5] ameliorating their properties and reducing the cost of the final sorbent. These adsorbents are also environmentally friendly [2,6,7].

* Corresponding author.

A part of the paper was presented at the 13th International Conference on Environmental Science and Technology (CEST 2013), September 5–7, 2013, Athens, Greece.

The aim of this work is the study of the removal of MB dye from aqueous solutions using new adsorbents such as modified zeolite, hematite, clinoptilolite, commercial activated carbon and modified zeolite-activated carbon in two different proportions (50/50 w/w and 20/80 w/w modified zeolite/carbon).

2. Materials and methods

2.1. Materials

Zeolite (CL) and commercial activated carbon (CB) derived from S&B (Attiki, Greece, 14564) and Merck (Attiki, Greece, 15123) companies, respectively. Hematite (HM) was produced using as raw materials $\text{Fe}(\text{NO}_3)_3 \cdot 9\text{H}_2\text{O}$, KOH, CH_3COOH and combined with clinoptilolite only for the preparation of modified zeolite in twice distilled water [8]. Modified zeolite (H-CL) derived from a ratio of zeolite/hematite equal to 1:2 w/w. Modified zeolite and commercial activated carbon in a proportion of 50/50 w/w (H-CL-CB1) and 20/80 w/w (H-CL-CB2) were also prepared. CL, CB, HM, H-CL-CB1 and H-CL-CB2 were ground and sieved to yield grains with a diameter less than 250 μm .

An aqueous solution of MB dye was used as adsorbate in 10 different concentrations, that is, 0.5, 1.0, 1.5, 2.0, 2.5, 3.0, 3.5, 4.0, 4.5 and 5.0 mg L^{-1} .

2.2. Characterization of the adsorbents

The Fourier transform infrared spectroscopic (FTIR) spectra of the adsorbents were obtained using a PerkinElmer spectrophotometer. All FTIR spectra were measured in transmission mode in the region of 4,000–400 cm^{-1} at a resolution of 4 cm^{-1} . Moreover, the salt addition method was employed to determine the point of zero charge (pzc) [9]. Specifically, an amount of 0.2 g of each adsorbent was added to 40 mL of 0.1 N KNO_3 in 10 falcon (50 mL) conical centrifuge tubes. The pH was adjusted using a pH meter to 2, 3, 4, 5, 6, 7, 8, 9, 10 and 11 (± 0.1 pH units) with 0.1 M HNO_3 and 0.1 M NaOH as needed in each falcon. They were then shaken for 24 h to reach equilibrium. Each resulting pH was measured and the initial pH (pH_0) in comparison with the difference between the initial and final pH values (ΔpH) was plotted. The initial pH at which ΔpH is zero was taken to be the pzc. Specific surface area (ssa) and pore size distributions (PSD) of the samples were measured by nitrogen adsorption–desorption isotherms, using a Micromeritics TriStar 3000 system, at liquid nitrogen temperature. All the samples were degassed at 250°C under vacuum for 18 h before analysis. For degassing we use the VacPrep 061 Degasser from Micromeritics. The ssa was calculated using the Brunauer–Emmett–Teller (BET) method. The total volumes of micropores and mesopores were calculated from the amounts of nitrogen adsorbed at $P/P_0 = 0.98$. The micropore volume and the external surface area were determined from the t -plot analysis. The PSD of the samples were calculated using the Barrett–Joyner–Halenda (BJH) method.

2.3. Effect of adsorbate initial concentration and contact time

Different MB initial concentrations, which ranged from 0.5 to 5.0 mg L^{-1} , were used in a proportion of adsorbent to

adsorbate solution equal to 0.1 g/10 mL at 20°C. After different time intervals, a specific amount of the solution was taken for examination using a VIS-spectrophotometer at 664 nm. The adsorbed amount (b_e) of the adsorbate onto the adsorbent at equilibrium was determined by the following equation:

$$b_e = \frac{(C_0 - C_e)V}{W} \quad (1)$$

where C_0 and C_e (mg L^{-1}) are the initial and final concentrations of MB, respectively, W (g) is the mass of adsorbent used and V (L) is the volume of the solution.

2.4. Adsorption isotherms

An amount of each adsorbent (0.02 g) was placed in 100 mL-plastic tubes, which were filled with solution with different MB initial concentrations, that is, 0.5–5 mg L^{-1} , during a batch operation. The experiments were done twice at three different temperatures, 20°C, 40°C and 60°C. The samples were equilibrated for 24 h and centrifuged for 10 min at 15,000 rpm. A specific amount of the solution was taken for examination using a VIS-spectrophotometer at 664 nm for MB. Adsorption isotherms indicate a graphical representation of the relationship between the adsorbed amount of adsorbate by the adsorbent (solid phase) and the remaining amount of adsorbate in the solution (liquid phase) at specific temperature and equilibrium conditions [10]. Langmuir and Freundlich isotherm models have been used to describe the experimental data. Moreover, according to thermodynamic study, the values of enthalpy ΔH° and entropy ΔS° were calculated from the Van't Hoff equation [11] and the Gibbs free energy ΔG° from the Gibbs relation at constant temperature [12].

2.5. Adsorption kinetic analysis

During a semi-batch operation, H-CL-CB1 or H-CL-CB2 was added in a 50-mL glass burette forming a column with dimensions equal to 1 cm of height and 1.15 cm of diameter. The weight of the column was equal to 0.4 g. Commercial activated carbon, modified zeolite, clinoptilolite and hematite were also used separately as adsorbents for comparison reasons. 25 mL of MB solution was passing through the burette with a constant velocity rate of 0.08 mL s^{-1} by proper regulation of the stopcock. When the total volume of MB solution passed through the column, an amount of MB solution was taken from the flask in order to be measured to the VIS spectrophotometer. Then, the burette was refilled again with the same MB solution from the Erlenmeyer flask. The process continued until MB solution of the flask reached equilibrium. The experiment was repeated twice and presented in Fig. 1.

The pseudo-first-order and the pseudo-second-order kinetic models were applied to the experimental data. The importance of diffusion in the adsorption process can be identified by the intraparticle diffusion model, which was described extensively by Weber and Morris [13].

3. Results and discussion

3.1 Adsorbents characterization

Two broad FTIR bands centered at 445, 528 and 1,035 cm^{-1} are characteristic for hematite (Fig. 2) while the band at 3,413 cm^{-1} corresponds to $-\text{OH}$ group and especially to triply coordinated functional groups (Fe_3-OH).

Bands centered at 1,616 cm^{-1} may possibly be assigned as O–H bending modes while the bands at 1,382 cm^{-1} were assigned to HCO_3^- [14]. The absorption peaks of clinoptilolite at 1,628, 3,221, 3,392 and 3,606 cm^{-1} are assigned to the combination and symmetric/asymmetric stretching modes of adsorbed water [15]. Vibrations of the Si–O(Al) bond caused by internal deformation (symmetric and antisymmetric) are revealed at the following range 1,043 and 786 cm^{-1} . A shoulder at 1,193 cm^{-1} corresponded to the asymmetric stretching vibration of the Si–O(Al) and Al–O(Si) bonds in zeolite. Weak bands, which were reported at 578 and 507 cm^{-1} , are assigned to the vibrations of aluminosilicate oxygen tetrahedral chains for clinoptilolite [16]. The bending vibration of Si–O–Si and O–Si–O can be seen at 449 cm^{-1} [17]. For iron-modified zeolite (H-CL), the bands at 1,625, 1,031 and 540 cm^{-1} shifted to lower wavenumbers than the bands in CL while the bands at 3,417, 790 and 461 cm^{-1} shifted to higher wavenumbers than the bands in CL. With the addition of hematite (HM), the bands of H-CL at 1,382 and 892 cm^{-1} were appeared. The two tripartite systems (H-CL-CB1, H-CL-CB2) presented higher bands at 1,647, 1,635, 1,041, 1,042 cm^{-1} , respectively, compared with the bands of CL. H-CL-CB1 system presented bands at 1,074, 875, 775, 460 cm^{-1} that were not found in H-CL-CB2 due to the increased amount of H-CL in H-CL-CB1 (50% w/w) compared with the respective amount of H-CL in H-CL-CB2 (20% w/w) showing that the FTIR spectrum of H-CL-CB1 presents similarities with H-CL. The FTIR analysis of commercial carbon has shown absorption peaks of C=O and OH [18]. Due to the presence of carbon, the functional groups in commercial carbon was difficult to be identified, due to their low concentration and proportion in comparison with the element of carbon and due to the spectrum background which is caused from the absorption of the black color of the carbon material [19].

According to Table 1, the two tripartite systems presented ssa equal to 558.85 and 708.31 $\text{m}^2 \text{g}^{-1}$ for H-CL-CB1 and H-CL-CB2, respectively. Raw materials presented lower ssa values than the tripartite systems, except for commercial carbon. From the t plot analysis, H-CL-CB2 appeared a micropore volume near to 0.18 $\text{cm}^3 \text{g}^{-1}$, micropore area equal to 448.35 $\text{m}^2 \text{g}^{-1}$ and external surface area equal to 259.96 $\text{m}^2 \text{g}^{-1}$. The adsorption average pore width was 30.09 Å with the BET method [21] and 24.79 Å with the BJH method [22], respectively. Moreover, H-CL-CB1 presented micropore volume, micropore area and external surface area equal to 0.14 $\text{cm}^3 \text{g}^{-1}$, 351.56 $\text{m}^2 \text{g}^{-1}$ and 207.29 $\text{m}^2 \text{g}^{-1}$, respectively. The adsorption average pore width was equal to 31.39 Å (BET method) and 26.17 Å (BJH method). The type of hysteresis loop shows narrow slit pores including pores in the micropore region (Type IV isotherms, Fig. 3). Such isotherms are typical for mesoporous materials while the increase in adsorbate volume in the low P/P_0 region indicates the presence of micropores associated with mesopores [23].

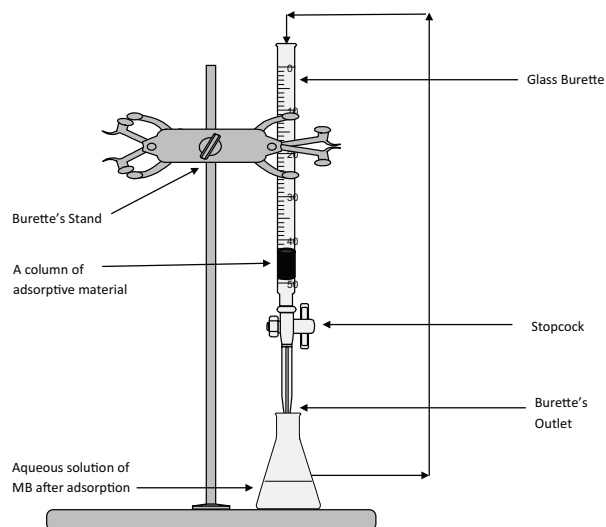


Fig. 1. Schematic representation of the removal of MB from aqueous solution using different adsorbents under a semi-batch operation using Advanced Chemistry Development, Inc. (ACD/Labs), ChemSketch freeware version, [54].

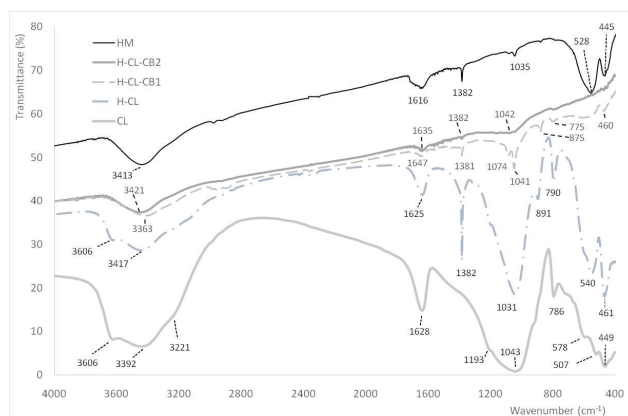


Fig. 2. FTIR spectra of all adsorbents (HM, CL, H-CL, H-CL-CB1 and H-CL-CB2).

Table 1

Experimental pzc and specific surface area (ssa) values for clinoptilolite (CL), hematite (HM), carbon (CB), modified zeolite (H-CL) and modified zeolite-activated carbon (H-CL-CB1, H-CL-CB2)

Adsorbents	pzc	ssa ($\text{m}^2 \text{g}^{-1}$)
HM	7.50–8.50 ^a	34.85
CL	8.88	29.40 ^b
CB	9.15	866.06
H-CL	7.30	38.43 ^b
H-CL-CB1	9.55	558.85
H-CL-CB2	7.92	708.31

^aAccording to Cornell and Schwertmann [20].

^bAccording to Ioannou et al., [8].

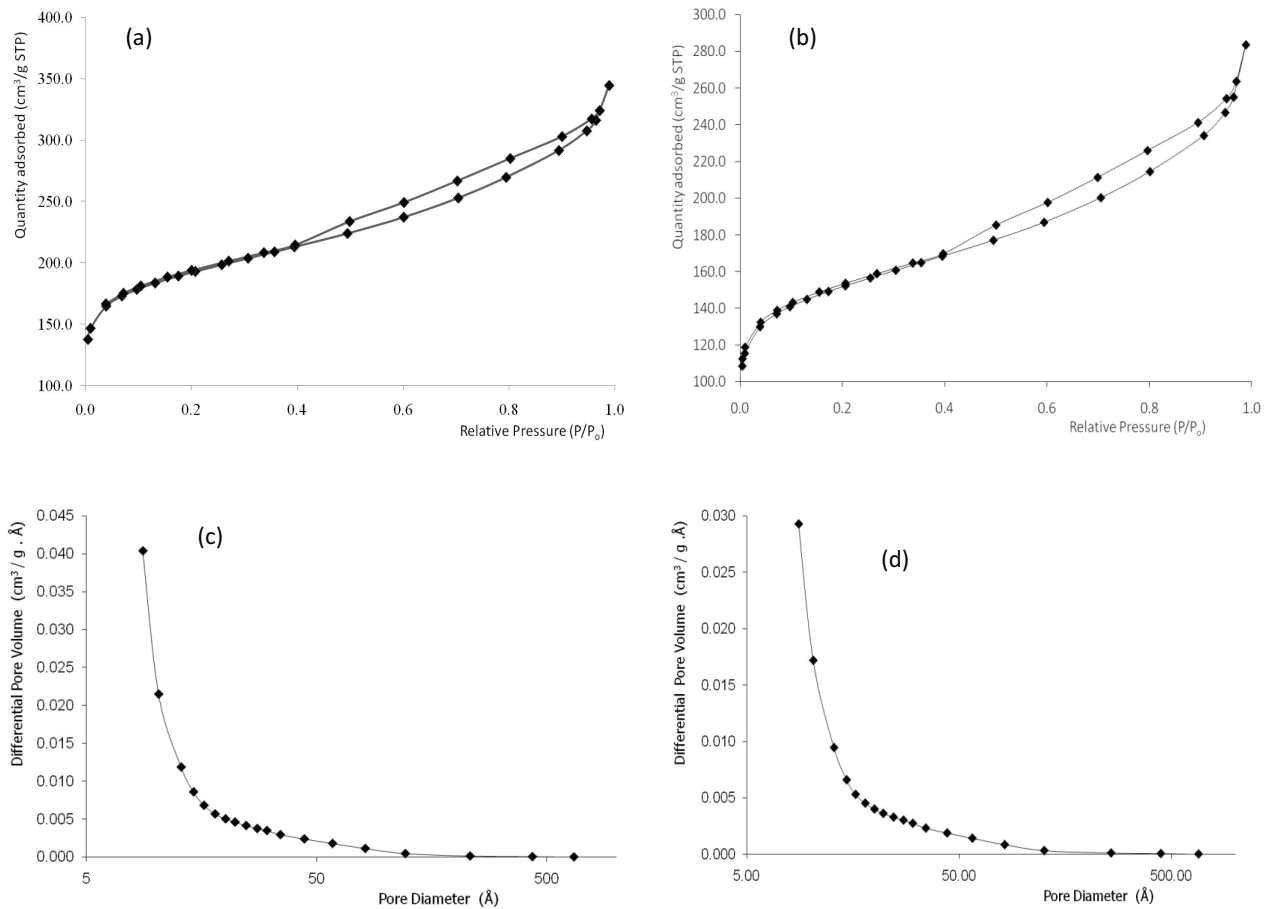


Fig. 3. Adsorption-desorption curves and differential pore volume of modified zeolite-commercial activated carbons [(a) and (c) H-CL-CB2, (b) and (d) H-CL-CB1].

The addition of each adsorbent to KNO_3 solution changes the pH values of each falcon tube, which was adjusted to specific values using HNO_3 or/and NaOH solutions, according to Fig. 4. In the pH range between 2.0 and 7.3, the ΔpH values were positive for H-CL adsorbent and then negative until pH 11.0. The maximum positive ΔpH value obtained at pH equal to 3.7. According to the two tripartite systems, the ΔpH values were positive in the pH range between 2.0 and 9.5 for H-CL-CB1 adsorbent and between 2.0 and 7.9 for H-CL-CB2 adsorbent. The maximum positive ΔpH value obtained at pH equal to 3.9 for H-CL-CB1 and at pH equal to 3.7 for H-CL-CB2. Raw materials presented positive ΔpH values in the pH 2.0–8.9 range for CL adsorbent and in the pH 2.0–9.2 range for CB adsorbent. The maximum positive ΔpH value obtained at pH equal to 3.6 for CL and to 4.1 for CB. The pH_{pzc} for carbons relies on the net total (internal and external) surface charge of particles. The commercial carbons, that were used, presented homogenous interfaces without additional treatments, that is, oxidation, activation or carbonization indicating a more homogenous distribution of the surface charges [24]. The pzc of all adsorbents were presented to Table 1. It seems that the two tripartite systems, that is, H-CL-CB1 and H-CL-CB2 differ to the pzc with the first one to be 9.55 and the second one 7.92. According to the definition of pH_{pzc} , that is,

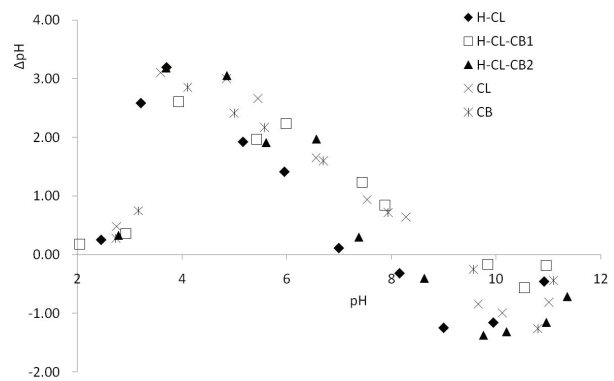


Fig. 4. The difference between the initial and final pH values (ΔpH) in comparison with the initial pH at 298 K and at different adsorbents, determined by the salt addition method.

the pH value where the surface material has a net neutral charge, pH values less than pH_{pzc} shows high concentrations of H^+ ions in the solution (H^+ -rich solution) resulting in positively charged surface of the adsorbent while pH values higher than pH_{pzc} shows low concentrations of H^+ ions in the solution (H^+ -poor solution) resulting in negatively

charged surface of the adsorbent. Adsorbents surface will have a positive charge at $\text{pH} < \text{pH}_{\text{pzc}}$ and thus be a surface on which anions may adsorb or a negative charge at $\text{pH} > \text{pH}_{\text{pzc}}$ and thus be a surface on which cations may adsorb [25]. Consequently, since the adsorption experiments of the two tripartite systems took place at highly basic pH values, negatively charged surfaces of H-CL-CB1 and H-CL-CB2 adsorb cations such as MB molecules.

3.2. Effect of initial concentration and contact time

Initial concentration plays an important role influencing adsorption process since it increases the amount of MB ions in the solution at a specific ratio of adsorbent to adsorbate solution. The effect of initial MB concentration on adsorption was studied in the range of $0.5\text{--}5.0 \mu\text{g mL}^{-1}$ (Fig. 5(a)).

According to the results, it seems that increasing the initial concentration of MB increases MB adsorption on each adsorbent for the specific range of MB concentrations. The increase of adsorption follows the order: $\text{HM} < \text{CL} < \text{CB} < \text{H-CL} < \text{H-CL-CB2} < \text{H-CL-CB1}$. Contact time is also a crucial parameter during the adsorption process. According to the results (Fig. 5(b)), it seems that when the initial MB concentration increases above $2.5 \mu\text{g mL}^{-1}$, MB adsorption on HM and CL will be stable after 120 h. All the other adsorbents (H-CL-CB2, CB, H-CL and H-CL-CB1) reached the equilibrium stage of MB adsorption until 6–6.5 h.

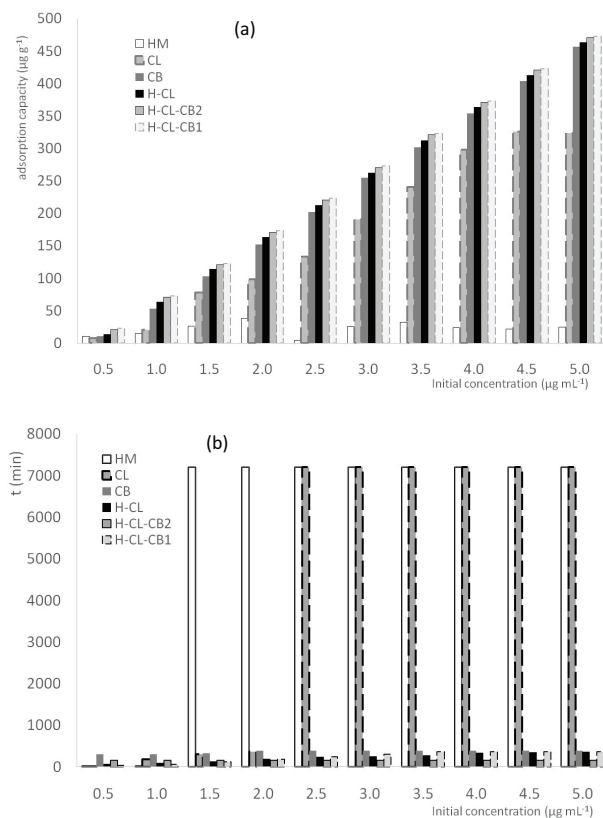


Fig. 5. Effect of (a) initial concentration and (b) contact time to the adsorption process.

3.3. Adsorption isotherms in a batch operation

In a batch operation (Figs. 6(a) and (b)), it seems that H-CL presented higher MB adsorption in equilibrium than CB for all examined temperatures. On the contrary, the raw materials of H-CL and especially HM showed the lowest MB adsorption ability (maximum adsorption at equilibrium from 17.140 up to 20.470 mg g^{-1} between 20°C and 60°C). According to Fig. 6(c), the tripartite systems have shown the highest MB adsorption in equilibrium, that is, 45.071 mg g^{-1} for H-CL-CB1 and 43.899 mg g^{-1} for H-CL-CB2 at 60°C . The adsorbed MB amount in equilibrium followed the order: $\text{HM} < \text{CL} < \text{CB} < \text{H-CL} < \text{H-CL-CB2} < \text{H-CL-CB1}$ for all temperatures.

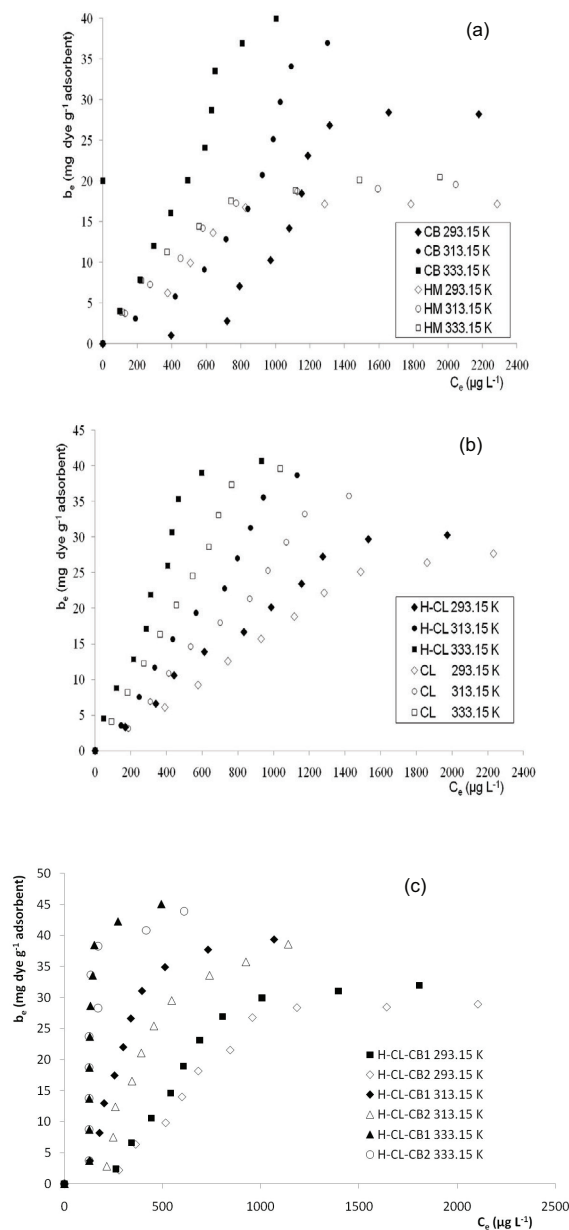


Fig. 6. Adsorption of MB in equilibrium per unit mass of adsorbent in correlation with the concentration of methylene blue in equilibrium for (a) CB, HM, (b) H-CL, CL and (c) H-CL-CB1, H-CL-CB2 at 20°C , 40°C , and 60°C .

Moreover, it seems that an increase in temperature led to an increase in MB adsorption for all adsorbents, for example, for equilibrium MB concentration of 930 μg L⁻¹, the adsorbed MB amount in equilibrium on H-CL was equal to 42.679 mg g⁻¹ at 60°C, 35.575 mg g⁻¹ at 40°C and 19.140 mg g⁻¹ at 20°C. Consequently, the increase of MB adsorption in equilibrium in comparison with temperature for the same adsorbent followed the order: 25°C < 40°C < 60°C.

The equilibrium adsorption isotherm is necessary to understand the adsorption system mechanisms. Langmuir equation supposes that the adsorption takes place at a specific adsorption surface. Langmuir isotherm is applied as follows:

$$b_e = \frac{b_m k_L C_e}{1 + k_L C_e} \text{ or } \frac{C_e}{b_e} = \frac{1}{k_L b_m} + \frac{1}{b_m} C_e \quad (2)$$

where b_e is the amount of MB adsorbed per unit mass of adsorbent in equilibrium (mg g⁻¹), C_e is the equilibrium MB concentration in the solution (mg L⁻¹), b_m is the amount of solute adsorbed per unit mass of adsorbent in forming a complete monolayer on the surface (monolayer capacity) and k_L is the Langmuir adsorption equilibrium constant related to the adsorption's energy [26].

Greater values of k_L indicate the affinity of adsorbent to adsorbate and imply strong bonding of MB ions. The dimensionless separation factor, R_L , was also evaluated using k_L values according to the following equation:

$$R_L = \frac{1}{(1+k_L C_0)} \quad (3)$$

where C_0 is the initial concentration of adsorbate. The values of R_L can be used for the interpretation of the adsorption type

showing that when $R_L = 0$ the adsorption is irreversible, $R_L > 1$ the adsorption is unfavorable and $0 < R_L < 1$ the adsorption is favorable [27].

Freundlich's empirical equation is based on the assumption that the adsorbent has a heterogeneous surface composed of different classes of adsorption sites. The Freundlich isotherm does not predict any saturation of the sorbent by the sorbate; thus infinite surface coverage is predicted mathematically, indicating multilayer sorption of the surface. Freundlich equation can be presented as:

$$b_e = k_F C_e^n \text{ or } \ln b_e = \ln k_F + n \ln C_e \quad (4)$$

where C_e (mg L⁻¹) is the equilibrium concentration of MB [28]. The linear plot obtained enables k_F and n to be determined. The relative adsorption capacity values were increased in accordance with the increase of temperature.

The experimental MB adsorption data were applied to Langmuir and Freundlich isotherms (Table 2). The applicability of these equations was quantitatively judged not only by correlation coefficient factor (r^2) but also by comparing the standard deviation ($\Delta b\%$) between the measured and modeled results of the adsorption in equilibrium (b_e). It was found that Freundlich equation, which shows multilayer adsorption, is more suitable for the description of MB adsorption isotherms onto CL, H-CL, H-CL-CB1 and H-CL-CB2. On the other hand, MB isotherms on HM and CB can be well fitted by the Langmuir equation, which shows monolayer adsorption. According to Table 2, an increase in temperature led to an increase in Freundlich constant, k_F , for CL, H-CL, H-CL-CB1 and H-CL-CB2. The values of n , which is indicative of the degree of surface heterogeneity, are lower than unity. Langmuir isotherm shows that the monolayer adsorption capacity of MB onto HM and CB was 25.316

Table 2

Best isotherm parameters of methylene blue adsorption from aqueous solutions onto (a) zeolite (CL), modified zeolite (H-CL), hematite (HM), commercial activated carbon (CB) and (b) modified zeolite-activated carbon (H-CL-CB1, H-CL-CB2) under a batch operation

(a)																
Adsorbents Isotherms T (K)	CB				CL				H-CL				HM			
	Langmuir				Freundlich				Freundlich				Langmuir			
	b_m	k_L	r^2	Δb (%)	k_F	n	r^2	Δb (%)	k_F	n	r^2	Δb (%)	b_m	k_L	r^2	Δb (%)
293.15	28.409	0.408	0.994	9.326	16.252	0.836	0.988	9.124	19.880	0.874	0.962	10.557	18.904	5.750	0.997	4.899
313.15	35.587	0.425	1.000	9.307	25.381	0.938	0.991	3.065	33.903	0.970	0.988	6.139	21.692	4.308	0.998	4.333
333.15	41.667	0.968	0.999	9.993	43.285	0.972	0.994	7.356	63.752	0.970	0.974	9.472	25.316	2.182	0.993	5.225

(b)										
Adsorbents Isotherms T (K)	H-CL-CB1					H-CL-CB2				
	Freundlich					Freundlich				
	b_m	k_F	n	r^2	Δb (%)	b_m	k_F	n	r^2	Δb (%)
293.15	31.920	25.227	0.926	0.938	31.34	28.930	20.755	0.871	0.939	31.14
313.15	39.330	58.369	0.845	0.939	29.83	38.610	43.610	0.846	0.932	31.37
333.15	45.070	120.301	0.971	0.922	60.82	43.910	82.006	0.805	0.926	60.80

Note: k_F units are (mg g⁻¹) (L mg⁻¹)^{1/n}, k_L units are L mg⁻¹ and b_m units are mg g⁻¹.

and 41.667 mg g⁻¹, respectively, at 60°C, higher than those obtained at 20°C and 40°C which were equal to 18.904 and 21.692 mg g⁻¹ for HM and 28.409 and 35.587 mg g⁻¹ for CB, respectively. It seems that all the separation factor values, R_L , were obtained between 0 and 1, showing that the adsorption of MB dye on HM and CB was favorable at the conditions being studied (Fig. 7). As MB dye initial concentration increased from 0 to 5 mg L⁻¹, the R_L values were found to decrease, indicating that the adsorption was more favorable at higher MB dye concentrations. Other researchers have shown similar results [29,30].

A comparison of MB adsorption capacities of various adsorbents is given in Table 3. It seems that H-CL-CB1, H-CL-CB2 and H-CL results (45.070, 43.899 and 42.679 mg g⁻¹, respectively) are quite similar to the adsorption capacity of activated *Rosa canina* seeds [31], nanomagnetite/heulandite/cross-linked chitosan (CCM) [35] and chitosan/sepiolite clay composite [39]. The MB adsorption capacity of H-CL-CB1 or H-CL-CB2 or H-CL is higher than other low-cost adsorbents such as activated carbons derived from different solid wastes or other clays and oxides [19,32,33,36–38,42,43,46]. In some cases, where polymers were added to minerals [45,46] the adsorption capacity is higher than those of the present work. Variation in MB adsorption capacity and affinity is mainly attributed to the differences in experimental condition conducted and properties of adsorbent such as ssa.

The values of enthalpy ΔH° and entropy ΔS° were calculated from the slopes and intercepts of the Van't Hoff plots of $\ln K$ vs. $1/T$ by fitting the experimental data to the equation [11]:

$$\ln K = \frac{\Delta S^\circ}{R} - \frac{\Delta H^\circ}{R} \frac{1}{T} \quad (5)$$

The Gibbs free energy ΔG° of specific adsorption was calculated from the equation:

$$\Delta G^\circ = \Delta H^\circ - T\Delta S^\circ \quad (6)$$

where R is the ideal gas constant and T (K) is the absolute temperature. The positive values of ΔH° and ΔS° indicate that the process is endothermic and thus the adsorption is

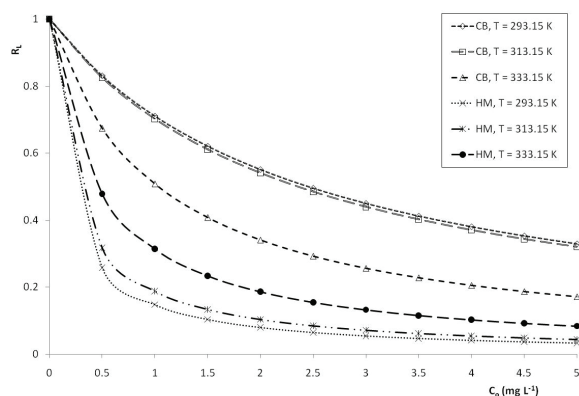


Fig. 7. Separation factor for MB onto HM and CB.

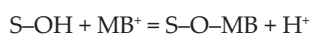
entropy driven while the negative values show that the adsorption is exothermic. The negative values of free energy change (ΔG°) indicate that the adsorption is spontaneous. Physical sorption and chemisorption may be indistinguishable in certain situations and in some cases a degree of both types of bonding is possible to be presented [29].

The values of adsorption equilibrium constant ($\ln K$) were obtained by plotting $\ln K_d$ vs. C_e and extrapolating C_e to zero. The intercept of the plot of $\ln K_d$ vs. C_e indicated the value of $\ln K$. Values of $\Delta H^\circ/R$ and $\Delta S^\circ/R$ were calculated from the slope and intercept of the plot of $\ln K$ vs. $1/T$, respectively (Fig. 8 and Table 4). The valuation of thermodynamic parameters provides an insight into the interaction between the surface of adsorbents and MB. The negative ΔG° indicated that the adsorption was a spontaneous process thermodynamically, and the value of ΔG° became more negative with the increase of temperature, showing that the adsorption process was more favorable to a higher temperature. The positive values of ΔH° indicate the endothermic nature of adsorption. Moreover, the sign of ΔS° indicates the direction of adsorption system. The ΔS° values were positive, indicating an increased disorder/randomness at the adsorbent/solution interface during MB adsorption. Other researchers have shown similar results [47].

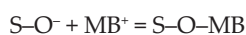
3.4. Influence of surface structure of adsorbents

According to Hegyesi et al. [48], the width, depth and thickness of MB are equal to 1.7, 0.76 and 0.33 nm, respectively. The results have shown an ssa, a micropore volume and a micropore area equal to 866.06 m² g⁻¹, 0.222 cm³ g⁻¹ and 545.175 m² g⁻¹ for CB, respectively (Table 1). Mercury porosimetry results showed that the majority of pore volume of CB (760 mm³ g⁻¹) corresponds to pore radius between 50 and 70 μ m [49]. These dimensions in comparison with the high ssa of CB allow the dye to have easy access within the porous structure of CB. In addition, the adsorption process is influenced by small amounts of surface functional groups present in CB [18]. On the other hand, due to the cationic properties of MB, its charge is delocalized throughout the chromophoric system, although it is probably more localized on the nitrogen atoms [27]. Other phenomena during MB adsorption may consist of hydrogen bonding formation, electron donor-acceptor mechanism due to the functional groups of S⁺ and N⁺(CH₃)₂ of MB which act as electron donors with electron acceptors functional groups of CB and π - π dispersion interaction mechanism between the aromatic ring of MB and the aromatic structure of the graphene layers [27].

The adsorption process of MB onto CL and H-CL depends mainly on the solution pH due to its influence to the non-permanent surface charge of colloids. Consequently, the pH-dependent adsorption of MB onto clay may be described as follows:



or



where S represents the active surface functional groups, S-OH and S-O⁻ refer to neutral and ionized surface

Table 3
Comparison of adsorption capacity of methylene blue on various adsorbents

Adsorptive materials	Adsorption capacity (mg g ⁻¹) ^a	References
Activated <i>Rosa canina</i> seeds	47.20	[31]
Activated carbons from hazelnut shells	8.82	[32]
Activated carbons from olive stones/novolac resin	5.44	[19]
Activated carbons from apricot stones	4.11	[32]
Activated carbons from walnut shells	3.53	[32]
Carbonized materials from olive stones/novolac resin	3.19	[33]
Activated carbons from almond shells	1.33	[32]
Corn cobs carbon activated by CO ₂	100.00	[34]
Corn cobs carbon activated by steam	75.50	[34]
Nanomagnetite/heulandite/cross-linked chitosan (CCM)	45.10	[35]
Modified zeolite-activated carbon (H-CL-CB1)	45.07	P.S.
Modified zeolite-activated carbon (H-CL-CB2)	43.90	P.S.
Modified zeolite with hematite	42.68	P.S.
Hematite	25.32	P.S.
NaOH-treated pure kaolin	20.49	[36]
NaOH-treated raw kaolin	16.34	[36]
SDBS-modified zeolite	15.68	[37]
Pure kaolin	15.55	[36]
SDS-modified zeolite	14.87	[37]
Raw kaolin	13.99	[36]
Zeolite	8.67	[37]
Pyrophyllite powder	3.71	[38]
Pickling pyrophyllite powder	3.83	[38]
Grinding pyrophyllite powder	3.94	[38]
Pickling-grinding pyrophyllite powder	4.24	[38]
Chitosan/sepiolite clay composite	40.99	[39]
Montmorillonite clay modified with iron oxide	71.12	[40]
Kaolin	52.76	[41]
Raw ball clay	25.01–34.65	[42]
Modified ball clay	62.50–100.00	[42]
Surface-modified clay	30.92	[43]
Raw clay	23.13	[43]
Natural clay mineral	62.5–100.0	[44]
(MMA-co-MMA)/SiO ₂ [H _{MMA}]	85.33	[45]
(MMA-co-HPMA)/SiO ₂ [H _{HPMA}]	87.37	[45]
PProDOT/MnO ₂	13.94	[46]

^aThe range in maximum adsorption capacities (MAC) for specific materials refers to MAC that correspond to different experimental temperatures.

hydroxyl functional groups. The ssa of CL and H-CL are 29.400 and 38.430 m² g⁻¹, respectively [8]. The micropore and mesopore volumes of these adsorbents are equal to 6.500 × 10⁻³ and 9.238 × 10⁻³ cm³ g⁻¹ for CL and 6.477 × 10⁻³ and 2.830 × 10⁻² cm³ g⁻¹ for H-CL [8]. Consequently, MB may enter into CL and H-CL, as indicated by the PSD of the adsorbents. From the analysis, it seems that the presence of an iron oxide such as hematite in zeolite surface increases the ssa of zeolite and consequently porosity. According to batch operation analysis, it seems that H-CL presented better adsorption

capacity than its raw materials due to the surface modification of zeolite with an iron oxide.

The tripartite systems such as H-CL-CB1 and H-CL-CB2 will present both the properties of commercial carbon and modified clay minerals. The adsorption average pore width is around 25 Å (BJH method) or 30 Å (BET method) for the tripartite systems while their ssa lie between 558.85 m² g⁻¹ for H-CL-CB1 and 708.31 m² g⁻¹ for H-CL-CB2 (Table 1). Moreover, according to FTIR analysis (Fig. 2), it seems that the functional groups of the two systems appeared in higher

The pseudo-second-order kinetic model can be expressed as follows:

$$\frac{t}{b_t} = \frac{1}{k_2 b_e^2} + \frac{t}{b_e} \quad (8)$$

where k_2 ($\text{g g}^{-1} \text{min}^{-1}$) is the equilibrium rate constant of pseudo-second-order adsorption. The slope of the plot of t/q_t vs. t was used to determine b_e and then from the intercept, k_2 was calculated.

The applicability of the data was further validated by the normalized standard deviation, Δb (%), which is defined as:

$$\Delta b(\%) = 100 \sqrt{\frac{\sum [(b_{\text{exp.}} - b_{\text{theor.}}) / b_{\text{exp.}}]^2}{N - 1}} \quad (9)$$

where N is the number of data points, $b_{\text{exp.}}$ and $b_{\text{theor.}}$ (g g^{-1}) are the experimental and calculated adsorption data, respectively. The higher is the correlation coefficient constant, r^2 , and the lower is the normalized standard deviation, Δb (%), the better will be the goodness of fit.

Adsorption kinetics is usually controlled by different mechanisms such as diffusion [50]. The intraparticle diffusion model can be defined as:

$$b_t = k_{\text{id}} t^{0.5} + C \quad (10)$$

where b_t is the amount adsorbed at time t , C is the intercept and k_{id} ($\text{g g}^{-1} \text{min}^{-0.5}$) is the intraparticle diffusion rate constant. If the regression of b_t vs. $t^{0.5}$ is linear and passes through the origin, then intraparticle diffusion is the sole rate-limiting step. Otherwise other mechanism along with intraparticle diffusion is also involved.

Since the nature of intraparticle diffusion plot confirms the presence of both film and pore diffusion, it is necessary to analyze the kinetic data using Boyd kinetic expression [51,52] so as to predict the actual slow step involved as follows:

$$1 - F = \frac{6}{\pi^2} \exp(-Bt) \text{ or } Bt = -0.4977 - \ln(1 - F) \quad (11)$$

where $F = b_t/b_o$, b_o and b_t are the amount of MB adsorbed at infinite time and at any time t , F represents the fraction of solute adsorbed at any time t and Bt is a mathematical function of F . The calculated B values were used to calculate the effective diffusion coefficient, D_e using the relation:

$$B = \pi^2 D_e / r^2 \quad (12)$$

where r represents the radius of the particle assuming spherical particles.

H-CL-CB1 and H-CL-CB2 were used as filters in a semi-batch operation representing better a semi-industrial scale operation. According to the results (Fig. 9(a)), H-CL-CB1 presented the highest percentage of MB adsorption (98.970% at 57 min) while H-CL-CB2 a percentage of MB adsorption equal

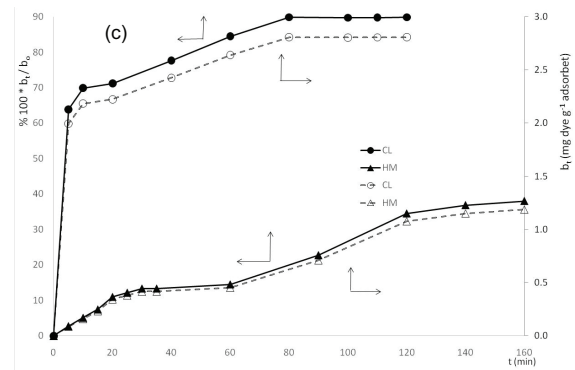
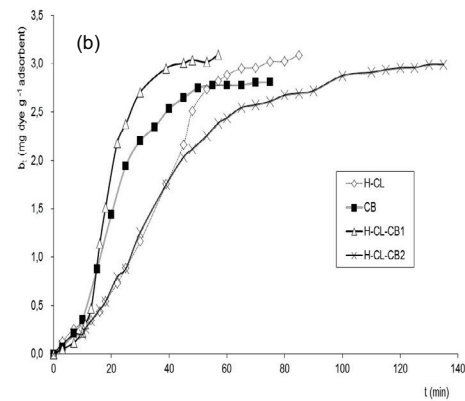
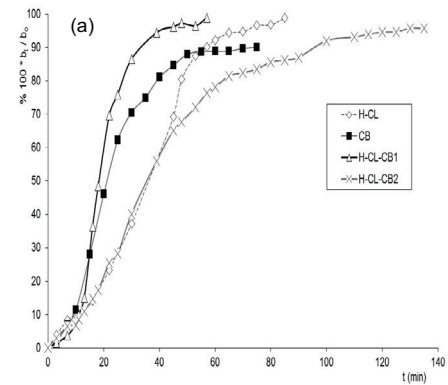


Fig. 9. Adsorption percentage (%) and adsorption amount (mg dye g^{-1} adsorbent) of MB from its aqueous solutions vs. time, t , using (a) and (b) CB, H-CL, H-CL-CB1, H-CL-CB2 and (c) CL, HM under a semi-batch process.

to 76.320% at 57 min. CB and H-CL followed intermediate values, that is, 88.800% and 90.240% at 57 min, respectively. According to Fig. 9(c), it seems that HM presented the lowest percentage of MB adsorption, that is, 38.045% while CL presented values equal to 89.886% after 100 min. The percentage of MB adsorption from aqueous solutions onto different adsorbents in a semi-batch operation follows the order: $\text{HM} < \text{CL} < \text{CB} < \text{H-CL-CB2} < \text{H-CL} < \text{H-CL-CB1}$. Moreover, the difference between MB adsorption onto H-CL-CB1 and H-CL-CB2 increased during time from 3 min at $0.471 \text{ mg dye g}^{-1}$ adsorbent up to 90 min at $2.953 \text{ mg dye g}^{-1}$ adsorbent (Fig. 9(b)). MB adsorption on CB was higher than H-CL for the first 50 min

and then H-CL presented better MB adsorption capacity than CB until they reached equilibrium. Comparing H-CL-CB2 with CB, it seems that until the first 80 min the adsorption percentage of CB was higher than H-CL-CB2 but then H-CL-CB2 continued to adsorb MB ions reaching at equilibrium at higher adsorption percentage values.

During the semi-batch application, kinetic parameters were also examined for the new tripartite systems (H-CL-CB1, H-CL-CB2) and compared with their raw materials (H-CL and CB). According to r^2 and Δb values applied to all kinetic models (Table 5(a)), the pseudo-second-order kinetic model fitted well the experimental MB adsorption data on H-CL and H-CL-CB1. The application of pseudo-second-order model has shown that H-CL-CB1 presented the highest value of k_2 , that is, the highest equilibrium rate constant, while H-CL-CB2 the smallest one. Pseudo-first-order equation presented relatively low r^2 and high Δb values showing its inappropriateness for analyzing the experimental data of the entire adsorption process. Involvement of intraparticle diffusion model on the evaluation of kinetic process as the sole mechanism was investigated. The values of b_i were plotted vs. $t^{1/2}$ leading to three different lines (Fig. 10(a)). The first one of these lines represents surface sorption, the second one is the

intraparticle diffusion and the third one is the final equilibrium stage. The parameters k , r^2 and Δb of intraparticle diffusion model were also calculated (Table 5(b)). According to the results, the adsorption of MB from aqueous solutions onto CB and H-CL-CB2 with the proportion of CB equal to 80% w/w presented high r^2 factors and low Δb values showing that intraparticle diffusion is the rate-limiting step. On the contrary, intraparticle diffusion mechanism was not appropriate for the adsorption of MB from aqueous solutions onto H-CL and H-CL-CB1 due to the low r^2 factors and high Δb values.

Since the double nature of intraparticle diffusion plot confirms the presence of both film and pore diffusion, it is necessary to analyze the kinetic data using Boyd kinetic expression so as to predict the actual slow step. The calculated Bt values were plotted against time, t , as shown in Fig. 10(b). It was observed that the plots were linear but do not pass through the origin confirming that film diffusion mainly governs the sorption process [50,52,53]. According to the results (Fig. 10(b)), Boyd expression is linear for CB and H-CL-CB2 with r^2 values greater than 0.974. The calculated effective diffusion coefficient, D_i ($\text{cm}^2 \text{s}^{-1}$), for all the adsorbents is presented in Table 5(c). It seems that CB presents higher effective diffusion coefficient than H-CL-CB2.

Table 5

Kinetic parameters (a), intraparticle diffusion parameters (b) and effective diffusion coefficient (c) of methylene blue adsorption from aqueous solutions onto modified zeolite (H-CL), commercial activated carbon (CB) and modified zeolite-commercial activated carbons (H-CL-CB1, H-CL-CB2) under a semi-batch operation

(a)

Adsorbents	$b_{e,\text{exp.}} \times 10^3$	Models							
		Pseudo-first-order				Pseudo-second-order			
		k_1	$b_{e,\text{theor.}} \times 10^3$	r^2	Δb (%)	k_2	$b_{e,\text{theor.}} \times 10^3$	r^2	Δb (%)
CB	2.813	0.083	5.323	0.960	98.780	10.092	3.921	0.956	22.434
H-CL	3.090	0.052	5.500	0.968	88.831	9.154	4.087	0.984	18.832
H-CL-CB1	3.093	0.089	5.767	0.957	98.159	12.994	4.190	0.980	16.784
H-CL-CB2	2.991	0.036	4.464	0.964	90.368	4.246	4.377	0.952	26.860

Note: $b_{e,\text{exp.}}$ and $b_{e,\text{theor.}}$ units are $\text{g dye}\cdot\text{g}^{-1}$ adsorbent, k_1 and k_2 units are $\text{g dye}\cdot\text{g}^{-1}$ adsorbent min^{-1} .

(b)

Adsorbents	Intraparticle diffusion model					
	First line			Second line		
	$k_{\text{id}} \times 10^4$	r^2	Δb (%)	$k_{\text{id}} \times 10^4$	r^2	Δb (%)
CB	3.632	0.863	68.021	6.550	0.987	6.743
H-CL	1.208	0.965	13.466	6.190	0.967	17.834
H-CL-CB1	1.519	0.877	66.769	9.862	0.931	19.708
H-CL-CB2	0.928	0.889	26.898	1.947	0.982	8.911

Note: k_{id} units are $\text{g dye}\cdot\text{g}^{-1}$ adsorbent $\text{min}^{-0.5}$.

(c)

Adsorbents	D_i ($\text{cm}^2 \text{s}^{-1}$)
CB	1.411×10^{-8}
H-CL	8.690×10^{-9}
H-CL-CB1	1.488×10^{-8}
H-CL-CB2	5.461×10^{-9}

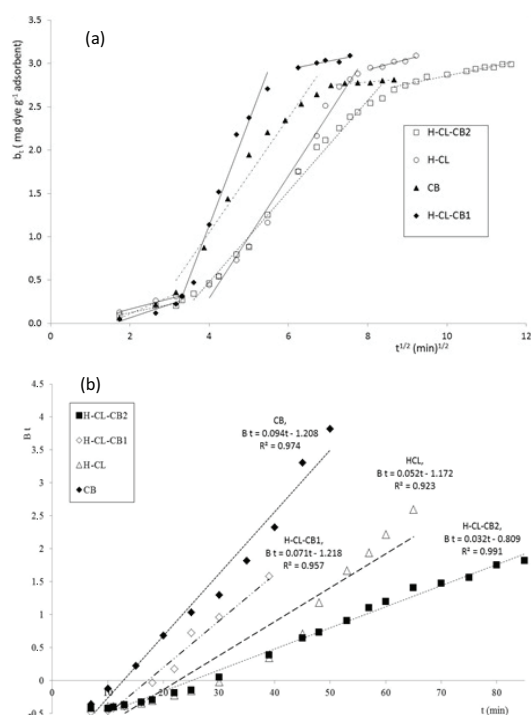


Fig. 10. (a) Intraparticle diffusion model and (b) Boyd's plot of methylene blue adsorption for CB, H-CL and H-CL-CB1, H-CL-CB2 under a semi-batch process.

H-CL-CB1 and H-CL-CB2 adsorbents appear a combination of adsorption properties of their raw materials. More specifically, H-CL-CB2, which consists of 20 w/w of modified zeolite (H-CL) and 80% w/w of CB presented similarities with CB. More specifically, the two adsorbents have shown similar ssa around 700 and 860 m² g⁻¹, respectively, and low concentrations of surface functional groups according to FTIR analysis indicating that the adsorption of MB from aqueous solutions onto H-CL-CB2 and CB do not depend on the surface functional groups of the materials but it followed the intraparticle diffusion model and more specifically film diffusion as the rate-limiting step (Table 5). On the contrary, H-CL-CB1, which consists of 50% w/w of CL and 50% of CB, presented similar behavior with H-CL due to the similarities in FTIR spectra with higher concentrations of functional groups and lower ssa than H-CL-CB2 and CB. This phenomenon was confirmed from Table 5 where MB adsorption onto H-CL and H-CL-CB1 followed the pseudo-second-order kinetic model indicating that chemisorption is the prevailing mechanism.

4. Conclusions

- According to FTIR analysis, it seems that FTIR spectra of H-CL-CB1 and H-CL are similar with high concentrations of surface functional groups. On the contrary, H-CL-CB2 presented very weak absorption bands indicating the low concentrations of surface functional groups.
- According to BET method, the ssa increases according to the order: CL < HM < H-CL < H-CL-CB1 < H-CL-CB2 < CB.
- The salt addition method led to the conclusion that the surfaces of H-CL-CB1 and H-CL-CB2 are negatively

charged having the ability to adsorb cations such as MB cations in aquatic environments.

- The adsorbed amount of MB at equilibrium onto HM, CL, H-CL, CB under a batch operation followed the order: HM < CL < CB < H-CL < H-CL-CB2 < H-CL-CB1 for temperatures 20°C, 40°C and 60°C, while thermodynamic analysis indicated that MB adsorption was endothermic and spontaneous.
- Equilibrium adsorption data were well fitted to the Langmuir isotherm model for HM and CB and to the Freundlich isotherm model for CL, H-CL, H-CL-CB1 and H-CL-CB2 under a batch operation.
- In a semi-batch operation, the rate-limiting step for MB adsorption from aqueous solutions onto CB and H-CL-CB2 is intraparticle diffusion mechanism and especially film diffusion while onto H-CL and H-CL-CB1 is the pseudo-second-order adsorption mechanism indicating that chemisorption is the prevailing mechanism.
- Modified zeolite-commercial activated carbon adsorbents in a proportion of 50/50 w/w H-CL/CB (H-CL-CB1) can be used as filters in semi-industrial scale operations combining the adsorption properties of carbons and zeolites.

References

- [1] S. Manna, D. Roy, P. Saha, D. Gopakumar, S. Thomas, Rapid methylene blue adsorption using modified lignocellulosic materials, *Process Saf. Environ. Prot.*, 107 (2017) 346–356.
- [2] M. Rafatullah, O. Sulaiman, R. Hashin, A. Ahmad, Adsorption of methylene blue on low cost adsorbents: a review, *J. Hazard. Mater.*, 177 (2010) 70–80.
- [3] P.B. Arab, T.P. Araújo, O.J. Pejon, Identification of clay minerals in mixtures subjected to differential thermal and thermogravimetry analyses and methylene blue adsorption tests, *Appl. Clay Sci.*, 114 (2015) 133–140.
- [4] S. Dardouri, J. Sghaier, A comparative study of adsorption and regeneration with different agricultural wastes as adsorbents for the removal of methylene blue from aqueous solution, *Chin. J. Chem. Eng.*, 25 (2017) 1282–1287.
- [5] A.H. Jawad, R.A. Rashid, M.A.M. Ishak, L.D. Wilson, Adsorption of methylene blue onto activated carbon developed from biomass waste by H₂SO₄ activation: kinetic, equilibrium and thermodynamic studies, *Desal. Wat. Treat.*, 57 (2016) 25194–25206.
- [6] Y. Miyoshi, K. Tsukimura, K. Morimoto, M. Suzuki, T. Takagi, Comparison of methylene blue adsorption on bentonite measured using the spot and colorimetric methods, *Appl. Clay Sci.*, 151 (2018) 140–147.
- [7] M.H. Dehghani, A. Dehghan, H. Alidadi, M. Dolatabadi, M. Mehrabpour, A. Converti, Removal of methylene blue dye from aqueous solutions by a new chitosan/zeolite composite from shrimp waste: kinetic and equilibrium study, *Korean J. Chem. Eng.*, 34 (2017) 1699–1707.
- [8] Z. Ioannou, C. Karasavvidis, A. Dimirkou, V. Antoniadis, Adsorption of methylene blue and methyl red dyes from aqueous solutions onto modified zeolites, *Water Sci. Technol.*, 67 (2013) 1129–1136.
- [9] T. Mahmood, M.T. Saddique, A. Naeem, P. Westerhoff, S. Mustafa, A. Alum, Comparison of different methods for the point of zero charge determination of NiO, *Ind. Eng. Chem. Res.*, 50 (2011) 10017–10023.
- [10] S. Rangabhashiyam, N. Anu, M.S. Giri Nandagopal, N. Selvaraju, Relevance of isotherm models in biosorption of pollutants by agricultural byproducts, *J. Environ. Chem. Eng.*, 2 (2014) 398–414.
- [11] E.S. Dragan, D.F.A. Loghin, Enhanced sorption of methylene blue from aqueous solutions by semi-IPN composite cryogels with anionically modified potato starch entrapped in PAAM matrix, *Chem. Eng. J.*, 234 (2013) 211–222.

- [12] C.-S. Zhu, L.-P. Wang, W.-B. Chen, Removal of Cu(II) from aqueous solution by agricultural by-product: peanut hull, *J. Hazard. Mater.*, 168 (2009) 739–746.
- [13] W.J. Weber Jr., J.C. Morris, Kinetics of adsorption on carbon from solution, *J. Sanit. Eng. Div.*, 89 (1963) 31–59.
- [14] Available at: http://minerals.gps.caltech.edu/files/Infrared_MIR/Minerals_From_JK/hematite.txt
- [15] J. Sá, J.A. Anderson, FTIR study of aqueous nitrate reduction over Pd/TiO₂, *Appl. Catal., B*, 77 (2008) 409–417.
- [16] K.B. Payne, T.M. Abdel-Fattah, Adsorption of arsenate and arsenite by iron-treated activated carbon and zeolites: effects of pH, temperature, and ionic strength, *J. Environ. Sci. Health, Part A*, 40 (2005) 723–749.
- [17] R.A. Razak, M.M. Al Bakri Abdullah, K. Hussin, K.N. Ismail, D. Hardjito, Z. Yahya Optimization of NaOH molarity, LUSI mud/alkaline activator, and Na₂SiO₃/NaOH ratio to produce lightweight aggregate-based geopolymer, *Int. J. Mol. Sci.*, 16 (2015) 11629–11647.
- [18] Z. Ioannou, J. Simitzis, Novolac Resin and Lignocellulosic Materials as Precursors for Carbonaceous Adsorbents, Seventh Hellenic Polymer Conference, Ioannina, Greece, 2008, 198–199.
- [19] Z. Ioannou, J. Simitzis, Adsorption of methylene blue dye onto activated carbons based on agricultural by-products: equilibrium and kinetic studies, *Water Sci. Technol.*, 67 (2013) 1688–1694.
- [20] R.M. Cornell, U. Schwertmann, *The Iron Oxides: Structure, Properties, Reactions, Occurrences and Uses*, New York, 1996, pp. 221–226.
- [21] S. Brunauer, P.H. Emmett, E. Teller, Adsorption of gases in multimolecular layers, *J. Am. Chem. Soc.*, 60 (1938) 309–319.
- [22] E.P. Barrett, L.G. Joyner, P.P. Halenda, The determination of pore volume and area distributions in porous substances. I. Computations from nitrogen isotherms, *J. Am. Chem. Soc.*, 61 (1951) 373–380.
- [23] S. Storck, H. Bretinger, W.F. Maier, Characterization of micro- and mesoporous solids by physisorption methods and pore-size analysis, *Appl. Catal., A*, 174 (1998) 137–146.
- [24] J.A. Menéndez, M.J. Illán-Gómez, C.A. León, Y. León, L.R. Radovic, On the difference between the isoelectric point and the point of zero charge of carbons, *Carbons*, 33 (1995) 1655–1659.
- [25] T. Mahmood, S.U. Din, A. Naeem, S. Tasleem, A. Alum, S. Mustafa, Kinetics, equilibrium and thermodynamics studies of arsenate adsorption from aqueous solutions onto iron hydroxide, *J. Ind. Eng. Chem.*, 20 (2014) 3234–3242.
- [26] M. Alkan, Ö. Demirbaş, S. Çelikçapa, M. Doğan, Sorption of Acid Red 57 from aqueous solution onto sepiolite, *J. Hazard. Mater.*, 116 (2004) 135–145.
- [27] A.M.M. Vargas, A.L. Cazetta, M.H. Kunita, T.L. Silva, V.C. Almeida, Adsorption of methylene blue on activated carbon produced from flamboyant pods (*Delonix regia*): study of adsorption isotherms and kinetic models, *Chem. Eng. J.*, 168 (2011) 722–730.
- [28] K.V. Kumar, S. Sivanesan, Equilibrium data, isotherm parameters and process design for partial and complete isotherm of methylene blue onto activated carbon, *J. Hazard. Mater.*, 134 (2006) 237–244.
- [29] E. Bulut, M. Özacar, I. Sengil, Equilibrium and kinetic data and process design for adsorption of Congo Red onto bentonite J. *Hazard. Mater.*, 154 (2008) 613–622.
- [30] K. Kumar, S. Sivanesan, Isotherm parameters for basic dyes onto activated carbon: comparison of linear and non-linear method, *J. Hazard. Mater.*, 129 (2006) 147–150.
- [31] A. Gurses, C. Dogar, S. Karaca, M. Acikyildiz, R. Bayrak, Production of granular activated carbon from waste *Rosa canina* sp. seeds and its adsorption characteristics for dye, *J. Hazard. Mater.*, 131 (2006) 254–259.
- [32] A. Aygun, S. Yenisoay-Karakas, I. Duman, Production of granular activated carbon from fruit stones and nutshells and evaluation of their physical, chemical and adsorption properties, *Microporous Mesoporous Mater.*, 66 (2003) 189–195.
- [33] Z. Ioannou, J. Simitzis, Production of carbonaceous adsorbents from agricultural by-products and novolac resin under a continuous countercurrent flow type pyrolysis operation, *Bioresour. Technol.*, 129 (2013) 191–199.
- [34] P.M.K. Reddy, P. Verma, C. Subrahmanyam, Bio-waste derived adsorbent material for methylene blue adsorption, *J. Taiwan Inst. Chem. Eng.*, 58 (2016) 500–508.
- [35] D.-W. Cho, B.-H. Jeon, C.-M. Chon, F.W. Schwartz, Y. Jeong, H. Song, Magnetic chitosan composite for adsorption of cationic and anionic dyes in aqueous solution, *J. Ind. Eng. Chem.*, 28 (2015) 60–66.
- [36] D. Ghosh, K.G. Bhattacharyya, Adsorption of methylene blue on kaolinite, *Appl. Clay Sci.*, 20 (2002) 295–300.
- [37] X. Jin, M. Jiang, X. Shan, Z. Pei, Z. Chen, Adsorption of methylene blue and orange II onto unmodified and surfactant-modified zeolite, *J. Colloid Interface Sci.*, 328 (2008) 243–247.
- [38] J. Zhang, Y. Zhou, M. Jiang, J. Li, J. Sheng, Removal of methylene blue from aqueous solution by adsorption on pyrophyllite, *J. Mol. Liq.*, 209 (2015) 267–271.
- [39] F. Marrakchi, W.A. Khanday, M. Asif, B.H. Hamed, Cross-linked chitosan/sepiolite composite for the adsorption of methylene blue and reactive orange 16, *Int. J. Biol. Macromol.*, 93 (2016) 1231–1239.
- [40] L. Cottet, C.A.P. Almeida, N. Naidek, M.F. Viante, M.C. Lopes, N.A. Debacher, Adsorption characteristics of montmorillonite clay modified with iron oxide with respect to methylene blue in aqueous media, *Appl. Clay Sci.*, 95 (2014) 25–31.
- [41] L. Mouni, L. Belkhir, J.-C. Bollinger, A. Bouzaza, A. Assadi, A. Tirri, F. Dahmou, K. Madani, H. Remini, Removal of methylene blue from aqueous solutions by adsorption on Kaolin: kinetic and equilibrium studies, *Appl. Clay Sci.*, 153 (2018) 38–45.
- [42] M. Auta, B.H. Hameed, Modified mesoporous clay adsorbent for adsorption isotherm and kinetics of methylene blue, *Chem. Eng. J.*, 198–199 (2012) 219–227.
- [43] S.J. Olusegun, L. Fernando de Sousa Lima, N.D.S. Mohalle, Enhancement of adsorption capacity of clay through spray drying and surface modification process for wastewater treatment, *Chem. Eng. J.*, 334 (2018) 1719–1728.
- [44] O.S. Omer, M.A. Hussein, B.H.M. Hussein, A. Mgaidi, Adsorption thermodynamics of cationic dyes (methylene blue and crystal violet) to a natural clay mineral from aqueous solution between 293.15 and 323.15 K, *Arabian J. Chem.*, 2017. <https://doi.org/10.1016/j.arabjc.2017.10.007>
- [45] H.S. Jamwal, S. Kumari, G.S. Chauhan, N.S. Reddy, J.-H. Ahn, Silica-polymer hybrid materials as methylene blue adsorbents, *J. Environ. Chem. Eng.*, 5 (2017) 103–113.
- [46] R. Jamal, L. Zhang, M. Wang, Q. Zhao, T. Abdiryim, Synthesis of poly(3,4-propylenedioxythiophene)/MnO₂ composites and their applications in the adsorptive removal of methylene blue, *Prog. Nat. Sci. Mater. Int.*, 26 (2016) 32–40.
- [47] S.K. Theydan, M.J. Ahmed, Adsorption of methylene blue onto biomass-based activated carbon by FeCl₃ activation: equilibrium, kinetics, and thermodynamic studies, *J. Anal. Appl. Pyrolysis*, 97 (2012) 116–122.
- [48] N. Hegyesi, R.T. Vad, B. Pukánszky, Determination of the specific surface area of layered silicates by methylene blue adsorption: the role of structure, pH and layer charge, *Appl. Clay Sci.*, 146 (2017) 50–55.
- [49] Z. Ioannou, J. Simitzis, Adsorption kinetics of phenol and 3-nitrophenol from aqueous solutions on conventional and novel carbons, *J. Hazard. Mater.*, 171 (2009) 954–964.
- [50] L. Ai, C. Zhang, F. Liaoa, Y. Wanga, M. Li, L. Mengb, J. Jiang, Removal of methylene blue from aqueous solution with magnetite loaded multi-wall carbon nanotube: kinetic, isotherm and mechanism analysis, *J. Hazard. Mater.*, 198 (2011) 282–290.
- [51] G.E. Boyd, A.W. Adamson, L.S. Myers Jr., The exchange adsorption of ions from aqueous solutions by organic zeolites: II. Kinetics, *J. Am. Chem. Soc.*, 69 (1947) 2836–2848.
- [52] S.K. Ghosh, A. Bandyopadhyay, Adsorption of methylene blue onto citric acid treated carbonized bamboo leaves powder: equilibrium, kinetics, thermodynamics analyses, *J. Mol. Liq.*, 248 (2017) 413–424.
- [53] K. Kumar, A. Kumaran, Removal of methylene blue by mango seed kernel powder, *Biochem. Eng. J.*, 27 (2005) 83–93.
- [54] ACD/ChemSketch, Freeware version 2015.2.5, Advanced Chemistry Development, Inc., Toronto, ON, Canada, www.acdlabs.com, 2015.